Differences in El Niño Response over the Southern Hemisphere

CAROLINA VERA

Centro de Investigaciones del Mar y la Atmósfera/Consejo Nacional de Investigaciones Científicas y Técnicas, and Departamento de Ciencias de la Atmósfera y los Océanos, Universidad de Buenos Aires, Buenos Aires, Argentina

GABRIEL SILVESTRI

Consejo Nacional de Investigaciones Científicas y Técnicas, Buenos Aires, Argentina

VICENTE BARROS

Departamento de Ciencias de la Atmósfera y los Océanos, Universidad de Buenos Aires, and Consejo Nacional de Investigaciones Científicas y Técnicas, Buenos Aires, Argentina

ANDREA CARRIL

Istituto Nazionale di Geofisica e Vulcanologia, Bologna, Italy

(Manuscript received 29 July 2002, in final form 29 August 2003)

ABSTRACT

Southern Hemisphere (SH) circulation conditions during austral springs of ENSO events are examined. Based on previous knowledge that SST variations over the subtropical south-central Pacific (SSCP) region are linked to differences among El Niño (EN) events, a stratification of the springs associated with EN events was performed according to SST conditions over the El Niño-3.4 sector and over the SSCP region. The EN events associated with cold conditions in the SSCP (WC) exhibit enhanced convection not only in the intertropical convergence zone over the central equatorial Pacific but also in the South Pacific convergence zone (SPCZ) extended southeastward into the subtropical regions. The resulting heating forcing intensifies a localized overturning cell, which is associated with an anomalous Rossby wave source in the central South Pacific extratropical region. Neither the Rossby wave source nor the associated wave pattern is evident during EN events associated with warm conditions in the SSCP and inactive SPCZ (WW).

The basic features that characterize the differences in the EN response over the South Pacific can also be identified through the analysis of the SPCZ activity over the central South Pacific. The fact that variations in SPCZ activity lead SST anomaly changes in the SSCP would indicate that the differences in the EN response over the SH might be mainly driven by atmospheric changes, which induces extratropical SST anomalies.

The differences in the circulation anomalies that characterize both types of EN response over the SH were further explored through the analysis of the activity of the three leading modes of circulation variability. The combined effect of the three leading patterns describes in some extent the intensification (weakening) of the cyclonic circulation anomaly observed over the southeastern Pacific in WC (WW), associated with an active (inactive) SPCZ. In particular, the interdecadal variability observed in the Pacific by many previous studies influences the circulation response to ENSO over the SH, mainly through changes in the activity of the SH annular mode.

1. Introduction

Several studies have extensively documented that a large part of the interannual variability of the Southern Hemisphere (SH) circulation is associated with El Niño–Southern Oscillation (ENSO). The atmospheric circulation response to ENSO events over the SH basically consists of a wave train that extends southeastward from the central tropical Pacific and it turns equatorward reaching South America (e.g., Karoly 1989). Actually, this response has elements of the second and third leading patterns of circulation anomaly variability over the SH on interannual time scales (Kidson 1999, among others).

The first leading pattern of circulation variability in the SH is related with zonally symmetric mass transfers between mid- and high latitudes (Fig. 1a). Kidson (1999) called this pattern, independent of ENSO variability, the high-latitude mode (HLM) while Thompson and Wallace (2000) called it the Antarctic Oscillation

Corresponding author address: Dr. Carolina Vera, CIMA, Pab. 2, 2do Piso, Ciudad Universitaria, 1428 Buenos Aires, Argentina.
E-mail: carolina@at.fcen.uba.ar

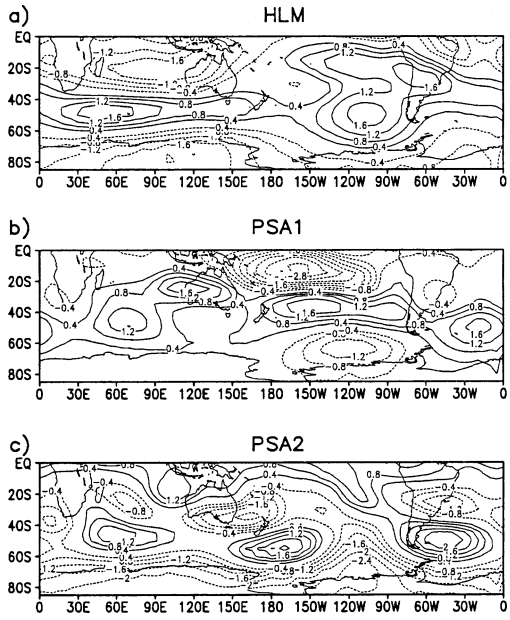

FIG. 1. (a) HLM, (b) PSA1, and (c) PSA2 patterns as identified from an EOF analysis for the streamfunction at $\sigma = 0.2$ described in section 5b. The meaning of PSA and HLM as well as the details of the EOF analysis are described in the text. Contour interval is 0.4 nondimensional units and the zero contour is omitted.

pattern. The second and third leading patterns correspond to the ''Pacific–South America'' (PSA) patterns (Mo 2000, and references therein). They are characterized by centers of anomalies extended from the Tropics and a wavenumber-3 structure at middle latitudes in quadrature with each other. The source region of the second leading pattern (PSA1, Fig. 1b) is located to the east of the dateline and that of the third leading pattern (PSA2, Fig. 1c) is in the vicinity of eastern Australia. Mo (2000) showed that PSA1 is associated with the low-frequency part of ENSO variability with dominant periods of around 40–48 months, while PSA2 is associated with the quasi-biennial component of ENSO variability with periods of around 26 months.

Wavelike response during El Niño (EN) or ENSO warm events is particularly noticeable over the circulation anomaly in the SH during the austral winter and more amplified during austral spring while this response becomes more zonally symmetric during the austral summer. Furthermore, during La Niña (LN), a wavelike response is also observed over the central South Pacific from the austral spring to the fall although they are not exactly the reverse of those associated with warm events (Kiladis and Mo 1998).

The global atmospheric climate signal associated with ENSO was described as an approximately linear response with anomalies during EN being the inverse of those during LN. In particular, Trenberth and Caron (2000) show that the PSA1-like pattern is evident in the regression fields associated with the Southern Oscillation, particularly during austral spring. On the other hand, Hoerling et al. (1997) analyzed the circulation anomaly patterns over the Northern Hemisphere (NH) associated with ENSO extremes and questioned the paradigm of an atmospheric system varying linearly with respect to the phases of such oscillation. They described an appreciable 35°-longitude phase shift of the circulation anomaly patterns between the warm and cold event over the NH, and found that the two wave trains appear to have different tropical origins. Performing numerical experiments, they concluded that the inherent nonlinearity in the tropical rain response between both ENSO phases might itself be responsible for the phase shift in the extratropical teleconnection patterns.

Extratropical circulation may significantly vary from event to event. This variation might not only be due to different conditions in both the ocean and the atmosphere at the Tropics and thus affecting Rossby wave sources, but also to differences in the conditions through which forced waves propagate to higher latitudes (Trenberth 1993). Performing numerical experiments, Kumar and Hoerling (1997) analyzed the variability in the circulation anomalies in the NH among different EN boreal winters. They argue that this variability does no appear to be a deterministic feature forced by SST anomalies, but that they might be primarily due to internal atmospheric variability.

Garreaud and Battisti (1999) documented the interdecadal (ENSO-like) signal on circulation anomalies in the SH, which is characterized by a strong annular structure at polar latitudes and a wavenumber-3 pattern at mid- and subpolar latitudes, a pattern somewhat different from the typical wavelike ENSO pattern.

The present study was originally motivated by the intention to see whether observed differences in the response of precipitation over South America to ENSO could be traced back to differences in the atmospheric and oceanic conditions over the South Pacific extratropics. Recently, Barros and Silvestri (2002, hereafter BS2002) explored the relationship between the interannual variability of global sea surface temperature (SST) and rainfall variability over southeastern South America (SESA) during the austral spring. They concluded that although SST at the equatorial region significantly modulates rainfall variability over SESA between EN, LN, and neutral years, it does not explain precipitation changes among different EN or among different LN years. In contrast, SST changes over the subtropical south-central Pacific (SSCP) between 170° and 120°W and 40° and 20°S (Fig. 3, bottom) may explain rainfall differences over SESA among years of equal ENSO phase. BS2002 showed that the ENSO signal on the atmospheric circulation anomalies in the SH might not only be linked to SST anomalies over the equatorial Pacific, but also to SST anomalies in the SSCP region.

Therefore, this paper explores to what extent the austral spring circulation in the SH during EN events, is associated to different oceanic and atmospheric conditions over the South Pacific. Emphasis has been placed

on the identification and characterization of the main wave train patterns. The paper is organized as follows. Section 2 describes data sources and analysis techniques. Section 3 discusses the SST anomaly variability at tropical and subtropical regions of the South Pacific during ENSO events, while the sea surface and atmospheric conditions during different EN event composites are described in section 4. Section 5 presents a discussion of the results and the concluding remarks are summarized in section 6.

2. Data and methodology

National Centers for Environmental Prediction–National Center for Atmospheric Research (NCEP–NCAR) reanalysis fields for the period 1958 to 2000 (Kalnay et al. 1996) are used to examine the circulation features. Kistler et al. (2001) provide a very detailed description of the NCEP reanalysis quality for the SH. In particular, there is an error in the reanalysis assimilation from 1979 to 1992. During that period, the Australian surface pressure bogus data mainly located over the Southern Oceans were read in 180° out of phase. While this error might affect daily analyses, it has a minimum influence on monthly mean fields. Questions might still remain about the quality of the reanalyses at high southern latitudes before satellite data become available (1979) and thus cautions should be taken in the results interpretation over middle and high latitudes of the SH. Nevertheless, reanalysis datasets such the one described are still the best dynamically consistent representation of the SH atmospheric circulation currently available.

The Global Sea Ice and SST dataset (GISST) from the United Kingdom Met Office (version 2.2; Rayner et al. 1996) on a 1° latitude × 1° longitude grid were used for the period 1958 to 1994 while the NCEP optimum interpolation SST analyses (Reynolds and Smith 1994) were considered afterwards (Trenberth et al. 2002). The GISST dataset exhibits some deficiencies in the temporal continuity anomalies after 1981 particularly at SH high latitudes (Hurrel and Trenberth 1999).

The present study focuses on the 3-month season that goes from October to December (hereafter referred to as OND). This season has the strongest ENSO signal in the circulation anomalies in the SH (Kiladis and Mo 1998) and in the subtropical South America precipitation (Montecinos et al. 2000; Grimm et al. 2000). Tropical zonal upper-level winds during OND are similar to those of the December to February (DJF) season (Schubert and Park 1991), with easterlies from Africa towards the dateline and westerlies elsewhere (Fig. 2a). Outside the Tropics, the circulation in the SH during OND resembles the conditions of the austral winter (Berbery et al. 1992) with a still present, but weaker subtropical jet over the western South Pacific Ocean.

The OND mean eddy streamfunction at upper levels (Fig. 2b) is very similar to that of the DJF season (Fig. 6 of Schubert and Park 1991) with north–south-oriented pairs of anticyclones at around 120°E and cyclones over the eastern Pacific and tropical Atlantic. A typical 1-wave pattern is evident at SH subpolar latitudes with an anticyclonic center located at around 60°S, 180°E. Over South America, the so-called Bolivian high, which is a dominant feature of the summer circulation, is already noticeable in the austral spring.

Global teleconnections of upper-level streamfunction anomalies are presented in the following sections and interpreted in terms of the quasi-stationary Rossby wave propagation theory. A useful diagnostic tool for representing three-dimensional propagation of stationary wave signal involves the calculation of the wave flux activity vectors defined by Plumb (1985). Following the Schubert and Park (1991) definition, the horizontal flux components that are applicable for quasigeostrophic stationary waves on a zonal flow are

$$F_\lambda = \frac{p}{2000a^2\cos\varphi}\left[\left(\frac{\partial\psi'}{\partial\lambda}\right)'^2 - \psi'\frac{\partial^2\psi'}{\partial\lambda^2}\right], \quad (1a)$$

$$F_\varphi = \frac{p}{2000a^2}\left(\frac{\partial\psi'}{\partial\lambda}\frac{\partial\psi'}{\partial\varphi} - \psi'\frac{\partial^2\psi'}{\partial\lambda\partial\varphi}\right), \quad (1b)$$

where p is pressure, φ is latitude, λ is longitude, a is the radius of the earth, ψ is the streamfunction, and primes denotes deviation from the zonal mean (the ''eddy'' component). Wave activity fluxes are parallel to the group velocity and their convergence indicates the piling up of the wave activity, while fluxes' divergence indicates its export (Plumb 1985). This approach has been extensively used in both model and observational studies (Brahmananda Rao et al. 2002 and references therein). Recently Barlow et al. (2001) used them as a diagnostic for identifying atmospheric teleconnections between the three primary modes of Pacific SST variability and U.S. hydroclimate. The authors mention that these fluxes essentially capture well the propagation of Rossby waves generated from a tropical heating source as realized in a linear model and thus they are useful for identifying the source region and propagation of stationary wave activity. However, considering that in the real atmosphere, tropical heating appears to affect the extratropics in a more complicated fashion and that the maintenance of the extratropical anomalies during ENSO involves strong synoptic eddy–mean flow interactions, the fluxes defined by Plumb (1985) might not necessarily help to identify the original physical forcing region.

Fluxes of wave activity associated with OND climatological eddy streamfunction exhibit regions of coherent zonal wave propagation from the central South Pacific towards South America (Fig. 2c). Schubert and Park (1991) show that there appears to be some cross-equatorial propagation of stationary waves from the Southern to the Northern Hemisphere in the eastern Pacific during austral summer.

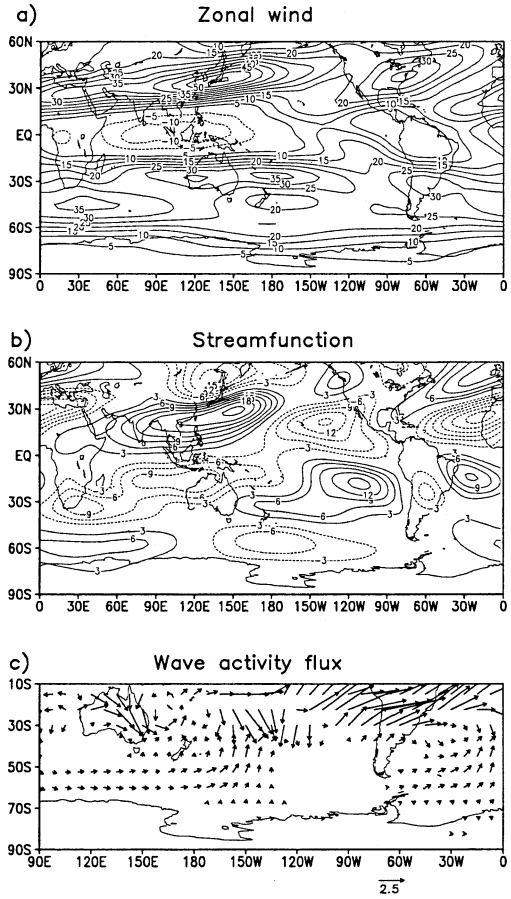

FIG. 2. Climatology for austral spring (OND) based on the years 1958–2000 of (a) 200-hPa zonal wind. Contour interval is 5 m s^{-1}. (b) Eddy streamfunction at $\sigma = 0.2$. Contour interval is 3.0×10^6 m^2 s^{-1}. (c) The wave activity flux vectors at $\sigma = 0.2$ based on the eddy streamfunction climatology. Vectors represent horizontal wave activity flux. A reference vector of 2.5 m^2 s^{-2} is shown at the lower right-hand side. The zero contour is omitted.

3. ENSO variability

Following BS2002, the relationships between SST anomalies at equatorial and subtropical regions of the South Pacific Ocean are explored through a scatter diagram, which relates SSTs in the El Niño-3.4 region (EN3.4) with those over the SSCP region (Fig. 3). As in BS2002, EN and LN events were considered as those defined by the Climate Prediction Center (available online at http://www.cpc.noaa.gov). An inverse relationship between SSTs in EN3.4 and those in SSCP is evident in Fig. 3. The correlation value between both SST anomaly time series is −0.69, significant at 95% level of an *F*-test. However, the relationship between the SST anomalies in both regions is small and not significant (−0.1), when only EN years are considered. Thus, the latter indicates that the SST anomaly changes at the SSCP region among EN cases are rather independent from those observed in the EN3.4 region. Because of that, EN events were classified into two main groups.

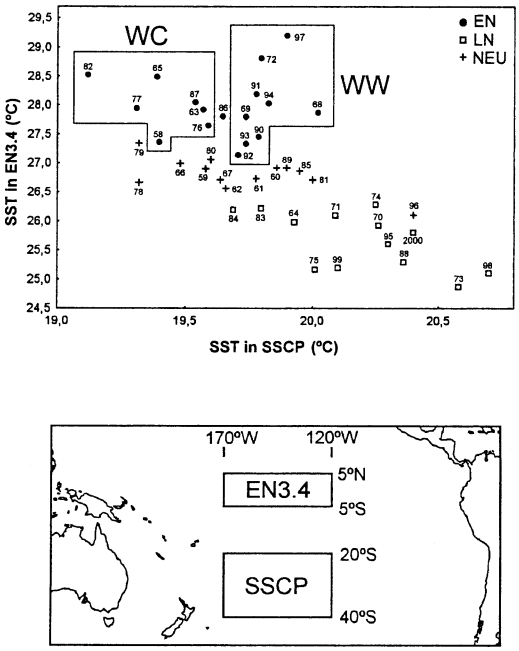

FIG. 3. (top) Scatter diagram between SST in EN3.4 and in the SSCP for OND. EN cases (dots), LN cases (empty squares), and neutral cases (crosses). The meaning of WC, WW is described in the text. (bottom) Ocean regions covered by EN3.4 and SSCP.

Events associated with warmest (W) equatorial SST and coldest (C) SST in the SSCP region were classified as the WC group, while the rest of EN events associated with warmer conditions at the SSCP region were included as the WW group.

SSTs in the SSCP region were considered warm or cold, depending on the sign of their difference with respect to the SST mean as computed among the corresponding EN years (Table 1). The EN event of 1986 was not included in any group as the SST value over the SSCP region for that year is 19.6°C and thus its difference against the SST mean for EN years was nearly zero. In the categorization of EN events, it resulted that WC and WW groups have almost identical SST conditions over the EN3.4 (Table 1).

When only LN events are considered, the correlation between the SST anomalies in both EN3.4 and SSCP regions has a significant value of −0.52. Therefore, the SST anomaly time series over the SSCP region does not seem to be a correct index to discriminate among different LN events.

In the following section, the ocean-surface and at-

TABLE 1. Means and std dev of SST (°C) in the EN3.4 and SSCP regions, for the groups of cases shown in Fig. 3.

	Cases		
	EN	WC	WW
EN3.4	28.0 ± 0.5	28.0 ± 0.4	28.0 ± 0.7
SSCP	19.6 ± 0.2	19.4 ± 0.2	19.8 ± 0.1

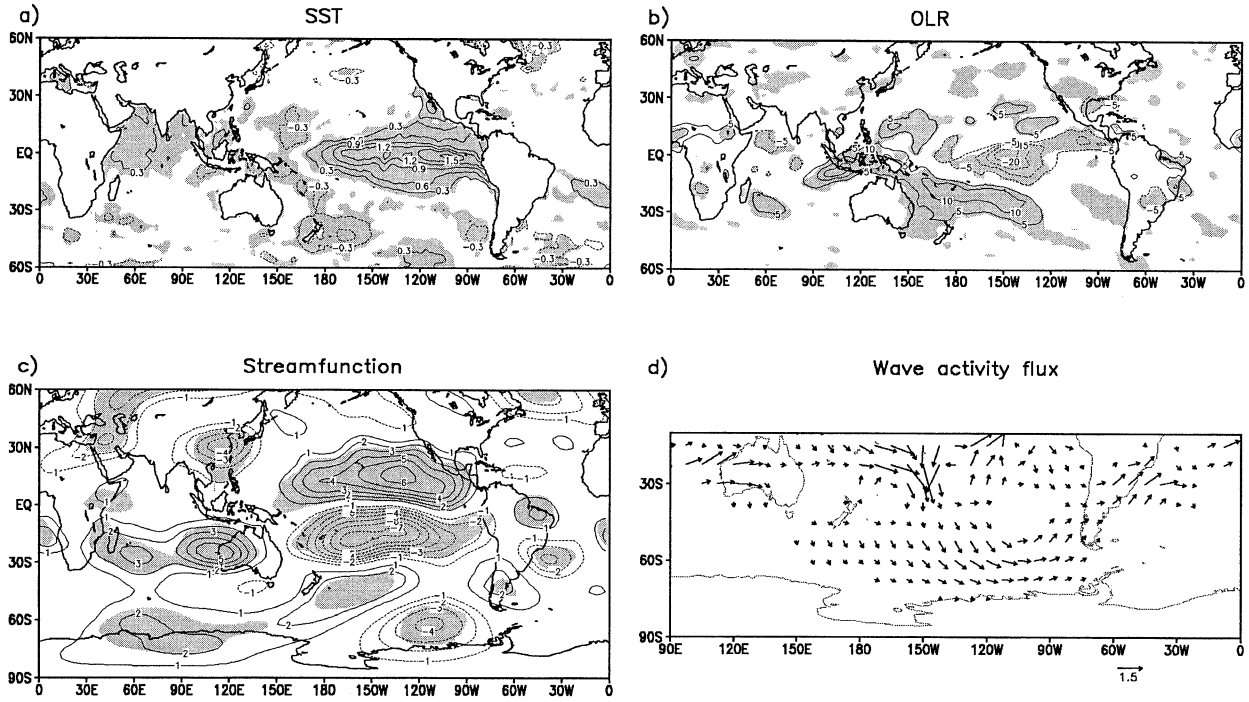

FIG. 4. Composites fields for EN events of (a) SST anomalies, (b) OLR anomalies, (c) streamfunction anomalies at $\sigma = 0.2$, and (d) corresponding wave activity fluxes. A reference vector of 1.5 $m^2\ s^{-2}$ is shown at the lower right-hand side. The contour interval is (a) 0.3°C, (b) 5 W m^{-2}, and (c) 1.0 $\times$ 10^6 $m^2\ s^{-1}$. The zero contour is omitted. Areas where values are statistically significant at the 95% level are shaded.

mospheric conditions of the two groups of EN events defined here are analyzed.

4. Atmospheric and oceanic conditions during El Niño

The EN composite anomalies were calculated with respect to the mean field of neutral years. The shading in the subsequent diagrams indicates areas where the value is statistically significant at the 95% level of a two-tailed *t* test assuming 1 degree of freedom per event. The corresponding field of SST anomalies exhibits the typical tongue of positive values along the equator while significant cool conditions prevail to the north of Australia and near New Zealand (Fig. 4a). Convection is enhanced at the equatorial central Pacific and inhibited over the Indonesian region and at the subtropical latitudes of the South Pacific, while the typical pattern of wet/dry conditions over SESA/northeastern South America (Ropelewski and Halpert 1987, among others) is also evident (Fig. 4b). The corresponding composite for upper-level streamfunction anomalies (Fig. 4c) shows the well-known pair of anomalous anticyclones straddling the equator while a wave train extends from the central equatorial Pacific and northwestern Australia, respectively, to the west of the Antarctic Peninsula and then northeastwards into South America. The intensity of the anticyclonic anomaly centered at around 70°S, 120°W is remarkable and consistent with the increased number of blocking events over that particular region during the spring and summer of EN events (Renwick 1998). Over South America, a cyclonic anomaly located at the southern tip of the continent, and an anticyclonic anomaly off the eastern coast, are observed, both favoring precipitation enhancement over SESA (Fig. 4b) as described by Grimm et al. (2000). Figure 4d shows the corresponding fluxes of stationary wave activity computed from eddy streamfunction anomalies. Considering the entire slowly varying component of the wave field, Karoly (1989) showed the significance of computing the wave activity from the field anomalies rather than from the total field. The largest magnitudes of stationary wave activity fluxes are in the tropical and subtropical regions of the central Pacific (Fig. 4d). Poleward fluxes come from both, the central equatorial Pacific and the western Australia regions to the SH subpolar regions (Fig. 4c). Over the southeastern Pacific, fluxes converge into the amplifying blocking ridge and reflect towards the equator contributing to maintain the anomaly circulation pattern over SESA.

The corresponding WC case (Fig. 5a) composites show warmer oceanic conditions at the eastern equatorial Pacific and colder ones at extratropical latitudes of both SH and NH, than in EN composites (Figs. 4a). Moreover, at the equator and east of the dateline, a more intense intertropical convergence zone (ITCZ) is connected to a band of enhanced convection extending toward the SH with a NW–SE orientation (Fig. 5b). The

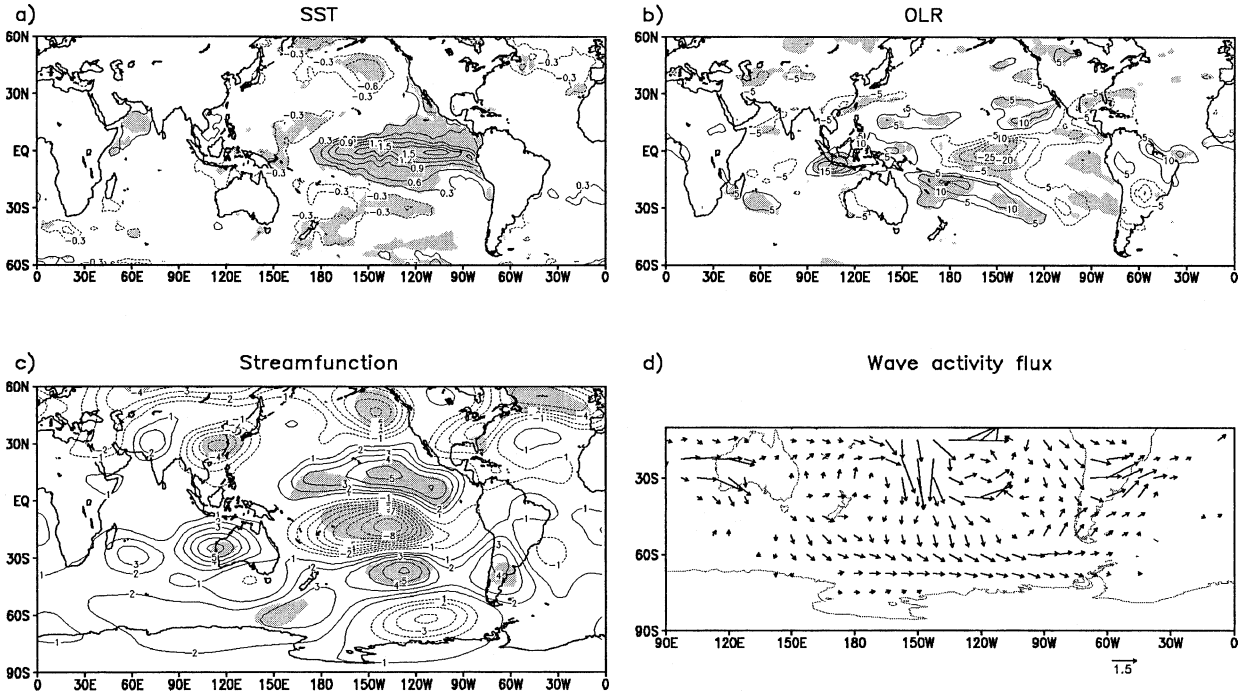

FIG. 5. As in Fig. 4 except for WC composites.

band indicates an extension of the South Pacific convergence zone (SPCZ) to the southeast of its climatological position during WC cases. In addition, the convective dipole, characteristic of EN events over the northeastern and southeastern regions of South America, is also more intense in the WC case.

The composite of upper-level streamfunction anomalies associated with WC (Fig. 5c) shows a stronger PSA1-like pattern compared to EN events (Fig. 4c). In particular, the cyclonic anomaly, observed in EN composites to the east of New Zealand, is significantly stronger and located eastward in WC while the trough over South America is also stronger and consistent with wetter conditions (Fig. 5b). Associated with these, there is a large (compared to EN) flux of stationary wave activity (Fig. 5d) over those two particular regions.

The WW composite shows a tongue of positive SST anomalies over the equator (Fig. 6a) weaker than WC with no evidences of cool oceanic conditions over the central South Pacific subtropics. On the other hand, weaker negative OLR anomalies are observed at the equator and larger positive anomalies in the subtropical South Pacific are more zonally oriented (Fig. 6b) as compared with those in WC composite (Fig. 5b).

A weakening of the upper-level circulation anomalies associated with WW (Fig. 6c) compared to WC (Fig. 5c) is evident over the southeastern Pacific and extratropical South America. Moreover, the maximum of the tropical anticyclonic anomaly is located around 30° farther west and there are no evidences of the subtropical cyclonic anomaly over the southeastern Pacific as it is in the WC composite.

Consistent with this, in WW there is no meridional propagation of stationary wave activity over the central South Pacific from tropical to extratropical latitudes (Fig. 6d), which is evident in both WC (Fig. 5d) and EN composites (Fig. 4d). Moreover, the wave activity flux from Australia towards SH high latitudes, which is observed in both cases is certainly weaker in WW.

The analysis of the differences between the WC and WW composite anomalies show that they are mainly concentrated in the central and eastern South Pacific and they are characterized by colder SSTs, an SPCZ southeastward extended and a stronger PSA1-like pattern (Fig. 7). Poleward fluxes of wave activity over the central Pacific also feature the main differences between both cases (not shown) while the troughing as well as the negative OLR anomalies over South America are different between the two groups of EN events, in agreement with BS2002 results. On the other hand, there are no significant differences over the western Pacific and surrounding subpolar regions. In the case of the subpolar anticyclonic anomaly there is some difference between both composites, but is not significant because of the large standard deviation observed among members of both WC and WW groups over the southeastern Pacific and surrounding Southern Oceans (not shown). Also, Sardeshmukh et al. (2000) show that this is one of the regions of the world that exhibits largest variability in the circulation response to EN.

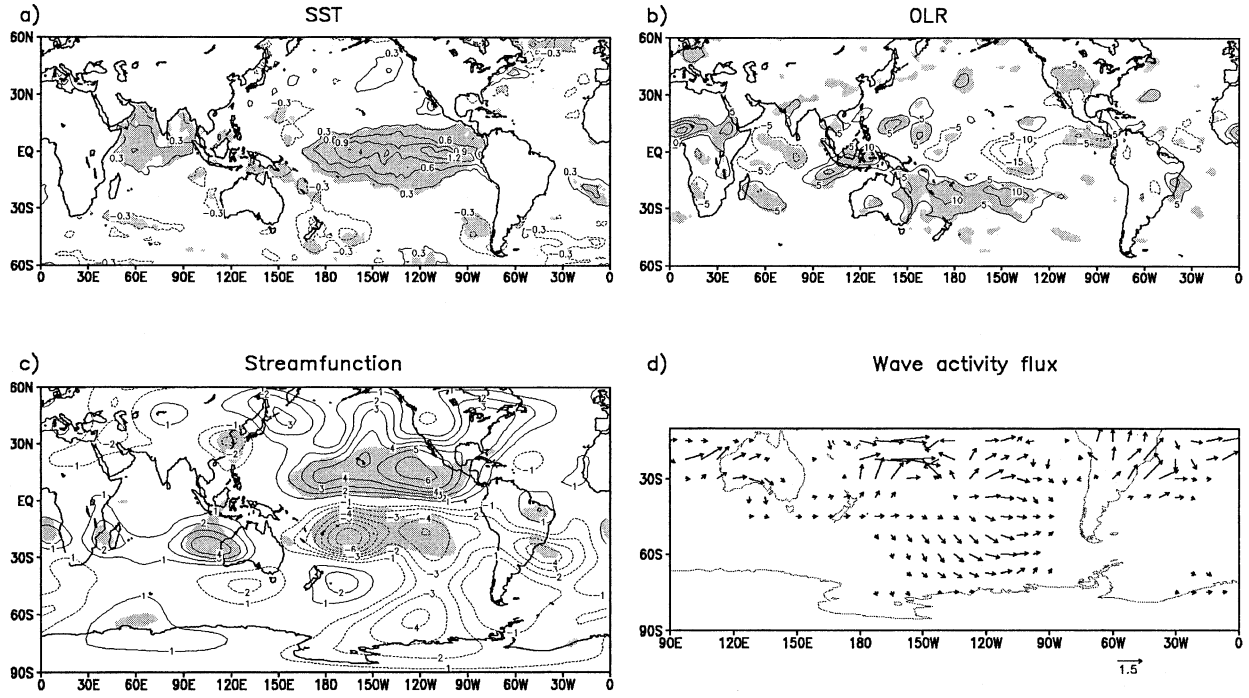

FIG. 6. As in Fig. 4 except for WW composites.

The fact that the PSA1-like pattern over the central South Pacific is stronger in WC than in WW can be illustrated through the analysis of the Rossby wave meridional propagation conditions over the central South Pacific. In fact, the meridional gradient of mean absolute vorticity in the WC case exhibits negative values eastward of New Zealand (not shown), thus inhibiting the meridional wave propagation there and constraining it more to the east (Fig. 5d).

Composites of divergent wind anomalies for WC, show (compared to WW) a more intense upper-level divergence region not only at the equator associated with the ITCZ but also along the NW–SE-oriented band of convection located at the subtropics associated with the diagonal portion of the SPCZ (Fig. 8a). A stronger downward branch of the overturning cell is also observed southwestward and the associated extratropical convergence should therefore be responsible for a large Rossby wave forcing (Rasmusson and Mo 1993). A typical diagnosis for such forcing of upper-tropospheric Rossby waves is

$$\overline{S} = \overline{-\nabla \cdot [\mathbf{V}_\chi(\varsigma + f)]} = \underbrace{\overline{-f\nabla \cdot \overline{\mathbf{V}_\chi}}}_{\text{(S1)}} - \underbrace{\overline{\varsigma\nabla \cdot \mathbf{V}_\chi} - \overline{\mathbf{V}_\chi \cdot \nabla(\varsigma + f)}}_{\text{(S2)}}, \quad (2)$$

where ($\bar{}$) denotes time mean, $\mathbf{V}_\chi$ is the divergent wind, ς is the relative vorticity, and S is the effective Rossby wave source derived from the time-averaged vorticity balance equation (Sardeshmukh and Hoskins 1988; Rasmusson and Mo 1993). Here, $\overline{S}$ was calculated for both, WC and WW, and for their difference (Fig. 8b). Rossby wave source anomalies appear where the anomalous latent heating extends outside of the equatorial belt into the subtropics, as indicated by the OLR anomalies (Fig. 5b). In agreement, Kodama (1999), among others, show that the trough and ridge patterns usually observed to the southwest and northeast, respectively, of the SPCZ are maintained by the strong diabatic heating released in the SPCZ. The contribution of the planetary vorticity-divergence stretching term [S1 of (2)] is quite similar to the total source anomaly field (Fig. 8c), confirming that this term is the dominant contributor to the Rossby wave source over the subtropical South Pacific.

5. Discussion

a. The South Pacific convergence zone

We have shown that SSTs of the SSCP region resulted in a good index to discriminate among EN events. This does not necessarily mean that they are the cause of the observed changes in the circulation response over the SH since SST anomalies in the SH extratropics might be induced by atmospheric circulation changes. Alexander et al. (2002) demonstrate that SST anomalies in the North Pacific are generated by alterations in the near-surface atmospheric conditions related to ENSO teleconnections. Then, is it possible to define an alternate index based on atmospheric conditions that describe similar differences among EN events?

The results presented in section 4 show that not only the convection at the equatorial Pacific, but also that

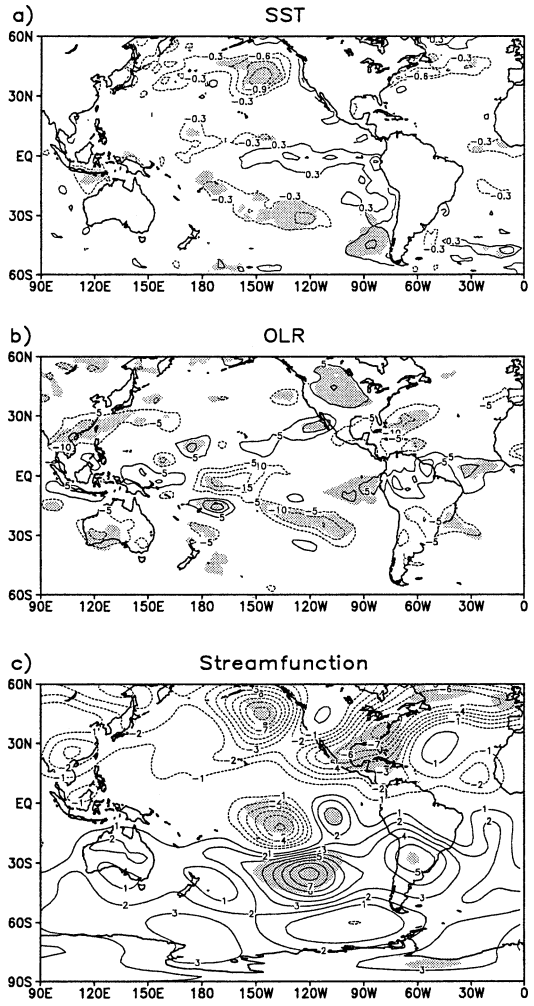

FIG. 7. Anomaly fields computed as the differences between WC and WW composite anomalies of (a) SST, (b) OLR, and (c) streamfunction at $\sigma = 0.2$. The contour interval is (a) 0.3°C, (b) 5 W m^{-2}, and (c) 1.0×10^6 m^2 s^{-1}. The zero contour is omitted. Areas where values are statistically significant at the 95% level are shaded.

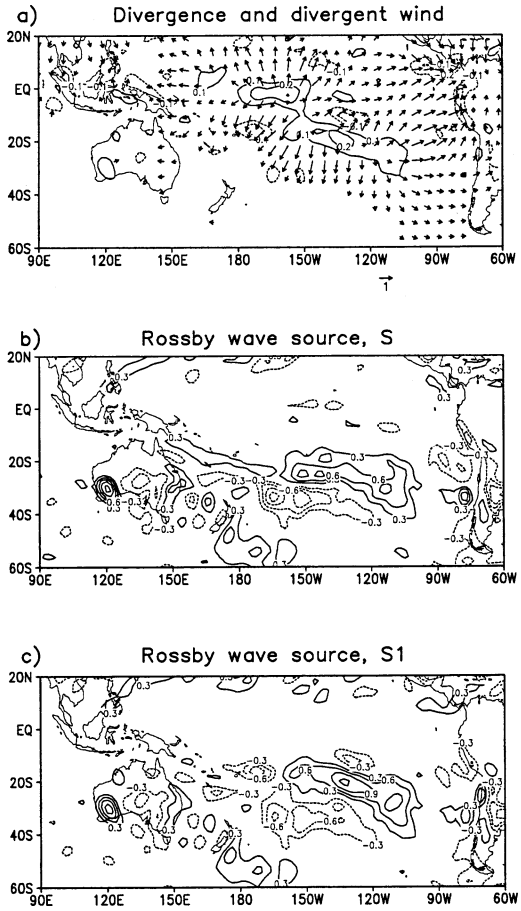

FIG. 8. Differences between WC and WW composite anomalies of (a) divergence and divergent winds, (b) Rossby wave source, and (c) the planetary vorticity-divergence term, at $\sigma = 0.2$. Contour interval is 0.1×10^{-5} s^{-1} in (a), and 0.3×10^{10} s^{-2} in (b) and (c). The zero contour is omitted.

associated with the SPCZ can be significantly different between WC and WW. Trenberth and Caron (2000) calculated the correlations of the Southern Oscillation index with annual and seasonal mean precipitation amounts and they found that the dominant pattern is one of shifts in the ITCZ and SPCZ, which tend to merge in the central Pacific during EN events. Our results confirm that the ITCZ shift is a common feature among different EN events, although the SPCZ intensification over the central Pacific seems to occur in some particular EN events and not in others (Figs. 5b, 6b). Performing studies with global circulation model outputs, Sardeshmukh et al. (2000) found that the remote circulation response to EN is stronger but also more *variable,* than the response to LN, a result that the authors suggest might be due to the greater variability of seasonal tropical rainfall during EN events.

In order to describe SPCZ changes over the central South Pacific, we defined an index based on the time series of the wind divergence anomalies at $\sigma = 0.2$ over the region (25°–15°S, 150°–125°W). In that particular area, the largest differences between WC and WW are observed in both OLR and upper-level divergence anomalies (Figs. 7b, 8a, respectively). A similar index based on OLR anomalies was also explored with similar results. Nevertheless, the SPCZ index based on the upper-level divergence anomalies was adopted because it seems to be more reliable than that based on ORL anomalies in depicting variations in years previous to the availability of satellite information.

The relationship between the EN3.4 SSTs and the SPCZ index is described through a scatter diagram (Fig. 9). A positive relationship between both series is evident with a significant correlation value of 0.41, indicating that in general warm (cold) ocean surface conditions at the equatorial Pacific are related with an enhanced (weakened) SPCZ over the subtropical central South Pacific, in agreement with Trenberth and Caron (2000). However, this correlation becomes small and nonsig-

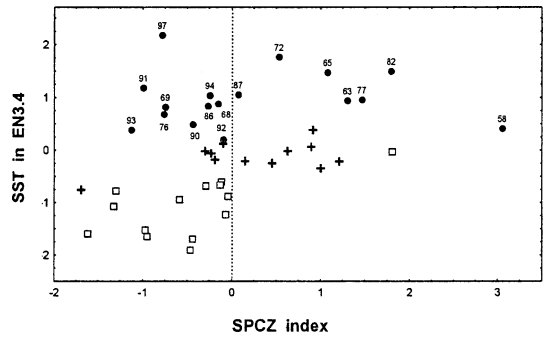

FIG. 9. Scatter diagram between standardized time series of SST in EN3.4 and the SPCZ index for OND. The SPCZ index definition is described in section 5a.

nificant (0.2) when only EN years are considered. It is evident from the scatter diagram that EN years can be associated with either both positive or negative anomalies of the upper-level wind divergence over the southeastern Pacific. On the other hand, all LN years are identified with upper-level convergence anomalies and there is no significant correlation between equatorial SST anomalies and the SPCZ index. In addition, neutral years can be associated with different SPCZ conditions, which might be indicating interannual variations of the convergence zone apparently unconnected with tropical Pacific SST forcing (Kidson et al. 2002).

The relationship between the SPCZ index and the SST anomalies over SSCP was also explored (Table 2). The simultaneous correlation between both series is −0.63, indicating that enhanced SPCZ conditions over the central Pacific are associated with cold ocean surface conditions at the subtropical South Pacific. This negative correlation significantly increases in magnitude to a value of −0.73 when only EN years are considered. On the other hand, there is no significant relationship between subtropical SST anomalies and SPCZ variations over central South Pacific during LN years (not shown). The analysis of the time-lagged correlations between both time series was also explored. When all years are considered, which includes EN, LN, and neutral years, austral winter changes of SST anomalies in the SSCP are statistically significant correlated with SPCZ changes during austral spring, while during the warm season, correlations are significant when the SPCZ index leads (Table 2a). On the other hand, when only EN years are considered, it is clear that SPCZ variations lead the SST anomaly changes in the SSCP by one season (Table 2b). It seems then that atmospheric conditions over the South Pacific would induce SST anomalies in the SSCP during EN events.

EN events were classified in two main groups based on the SPCZ index values in a similar way as it was done in section 3 considering the SST anomalies in the SSCP region. EN events associated with an enhanced SPCZ over the central South Pacific (positive SPCZ index) were grouped in the SPCZ+ case, while EN

TABLE 2. Time-lagged correlations between the SPCZ index and the SST anomalies over SSCP calculated (a) for all years (1958–2000) and (b) only among EN years. Values statistically significant at 95% are boldface.

a)

	SST anomalies in SSCP		
	JJA	OND	JFM
SPCZ index			
JJA	**−0.33**	−0.21	−0.23
OND	**−0.50**	**−0.63**	**−0.60**
JFM	−0.16	−0.23	−0.28

b)

	SST anomalies in SSCP		
	JJA	OND	JFM
SPCZ index			
JJA	−0.42	**−0.65**	−0.31
OND	−0.36	**−0.73**	**−0.59**
JFM	0.02	−0.25	**−0.59**

events associated with a weakened SPCZ (negative SPCZ index) were included in the SPCZ− case. A comparison between both EN event groupings (Figs. 3, 9) shows that essentially SPCZ+ (SPCZ−) gathers the same EN events as WC (WW). Although, there are some differences as follows: (i) 1972 event is included in SPCZ+ and not in WC, (ii) 1976 event is in WC and not in SPCZ+, and (iii) 1986 event is in SPCZ− while it is not included either in WC nor in WW.

Anomaly composites of atmospheric and SST fields were made for SPCZ+ and SPCZ− (not shown) and they very much resemble the features observed for WC and WW, respectively, as described in section 4. It can be thus concluded that both, changes in SST conditions in SSCP as well as SPCZ changes over the central South Pacific, are able to describe the main differences detected in the response to EN over the SH. It remains to be determined, however, which are the causes of those differences.

b. The leading modes of circulation variability in the SH

The circulation anomaly patterns showed previously for different EN composites, resemble some of the features of the leading modes of circulation in the SH, particularly of PSA1 and PSA2 (Fig. 1). However, to what extent are the circulation differences between WC and WW related to changes in the activity of the leading modes?

Figure 1 shows the patterns of the first three empirical orthogonal functions computed on the monthly mean streamfunction anomalies at $\sigma = 0.2$ over the SH (90°S–equator) for austral spring (October–December). Kidson (1999), among others, has explored the stability of these modes using reanalyzed fields. Recently Cai and Watterson (2002), through the analysis of climate model

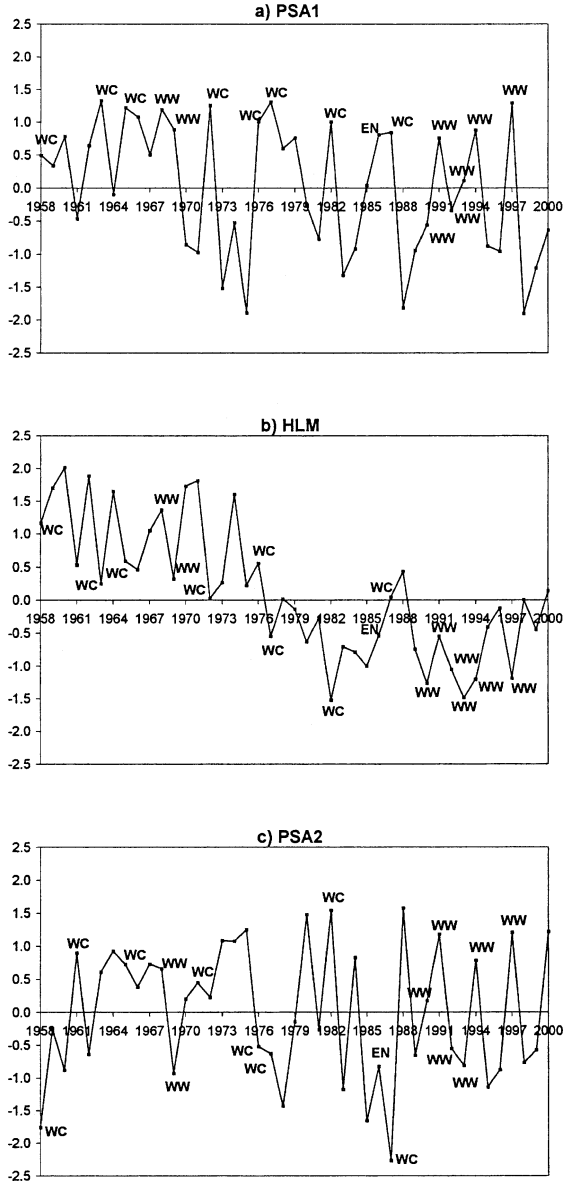

FIG. 10. Normalized principal components (time series) for (a) PSA1, (b) HLM, and (c) PSA2. Years associated with either WC or WW are marked.

simulations found that although the ENSO forcing projects mainly onto the PSA1 mode, the three leading modes can be generated by atmospheric internal dynamics alone, and that the ocean dynamics, air–sea interaction, and ENSO forcing are not essential.

The time series of the three leading modes are displayed in Fig. 10. The PSA1 time series exhibits considerable interannual variability highly correlated with ENSO (Fig. 10a), as previously identified by many authors (Mo 2000 and references therein). In particular, most of EN events regardless of whether they are grouped in WC or WW are associated with the positive phase of PSA1 (Fig. 1b). Although, the mean PSA1 amplitude associated with WC is around twice that for WW.

The main feature observed in the HLM time series (Fig. 10b) is the low-frequency change, with negative values after the middle seventies, which indicates heights decreasing over Antarctica and increasing at midlatitudes (Fig. 1a). The trend associated with the SH annular mode has been described by many authors although it still remains to be determined which is the primary causal mechanism (Thompson et al. 2000, and references therein). On the other hand, several works have described the ''regime shift'' of 1976/77 and related it with interdecadal climate variations of the ocean–atmosphere system in the Pacific (e.g., Graham 1994). Mo (2000) demonstrates that the circulation anomalies in the SH associated with the interdecadal variability can be explained as a mixture of both HLM and PSA1 signals. Trenberth et al. (2001) shows that a shift occurred in the EN3.4 SST anomalies around 1976/77 toward warmer and more EN-like conditions. The correlation between the EN3.4 SST anomalies and the HLM time series is negative although barely significant (-0.27). Around 75% of the WC (WW) cases occur before (after) the 1976/77 period and they are related with a positive (negative) phase of the HLM (Fig. 10b). Thus, the differences between WC and WW seem to be in some extent related to the interdecadal change that occurred in the middle seventies. That might explain why some remote regions like the North Pacific and North Atlantic, exhibit significant composite differences between both EN groups (Fig. 7). Zhang et al. (1997) showed that the SST signature in the interdecadal variability is very prominent in the North Pacific and the circulation signature resembles the Pacific–North American pattern.

The temporal variability of PSA2 (Fig. 10c) is mostly dominated by a quasi-biennial signal (Mo 2000). Although the correlation between the PSA2 time series and the EN3.4 SST anomalies is negligible, it increases to a significant value of 0.54 when only EN years are considered. Figure 10c shows that around half of EN events occur in association with the positive phase of PSA2, and there is no clear distinction between a specific PSA2 phase and the occurrence of EN events of either WC or WW type.

In order to quantify how much of the differences observed in the circulation anomalies between WC and WW (Fig. 7c) are accounted for by the activity of the three leading modes, the composites of the circulation anomalies, reconstructed considering only the contribution of the first three leading EOFs, were explored. Specifically, the streamfunction anomalies at $\sigma = 0.2$ were recomputed (Kutzbach 1967, among others), as

$$\psi'_R(\lambda, \varphi, t) = \frac{1}{3}\sum_{k=1}^{3} \mathrm{EOF}_k(\lambda, \varphi)\mathrm{PC}_k(t), \qquad (3)$$

where the EOF are the three eigenvectors associated

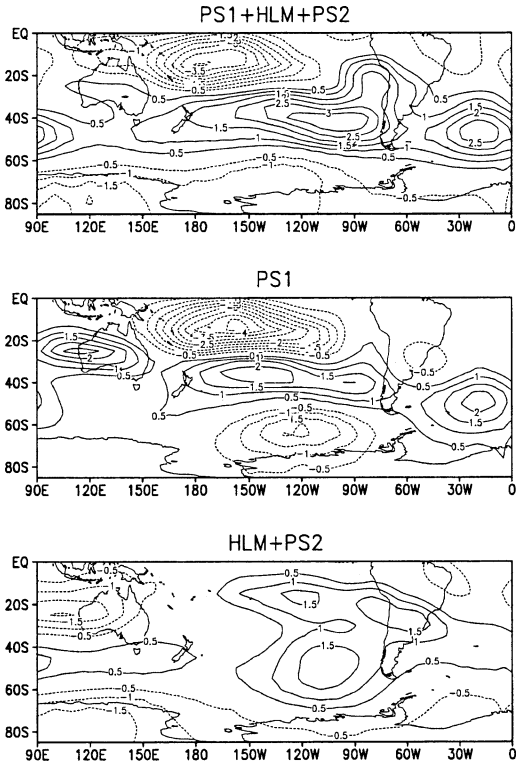

FIG. 11. (a) Differences between WC and WW composite anomalies of reconstructed streamfunction (ψ'_R). The definition of ψ'_R is described in section 5b. Contributions of (b) PSA1 and (c) HLM+PSA2 to ψ'_R differences exhibited in (a). Contour interval is 1.0×10^6 m^2 s^{-1} and the zero contour is omitted.

with HLM, PSA1, and PSA2, respectively (Fig. 1) and the PC are the corresponding temporal coefficients, which have their normalized versions depicted in Fig. 10. The reconstructed anomalies significantly account for around 80% of the total variance of the actual ones over the region (45°–35°S, 150°–110°W) that encompasses the location of the cyclonic center observed in the difference field between WC and WW composites (Fig. 7c). In particular, the PSA1, HLM, and PSA2 variability account for 60%, 16%, and 11%, respectively, of the total variance observed over that particular region, with only the PSA1 contribution being statistically significant. On the other hand, the contribution of PSA1, HLM, and PSA2 to the observed variance among EN events, are 41%, 65%, and 16%, respectively, with the first two contributions significant.

The difference of the ψ'_R composites between WC and WW (Fig. 11a) exhibits certain features of the observed differences (Fig. 7c). They are characterized by the anticyclonic anomaly over the tropical South Pacific, which is located in the reconstructed field farther west than observed, and by a band of cyclonic anomalies extended from the central South Pacific towards South America (Fig. 11a). The PSA1 contribution is in general stronger in WC than in WW (Fig. 11b), which is consistent with the ITCZ enhancement observed in WC compared to WW (Fig. 7b). On the other hand, the combined contribution of HLM and PSA2 (Fig. 11c) produces in WC (compared to WW) a weakening of the PSA1 anticyclonic anomalies at both tropical and subpolar latitudes and an intensification of the PSA1 cyclonic signal at midlatitudes.

6. Concluding remarks

The differences in the response to EN over the SH were analyzed in this paper. It was found that a group of EN events (WC) are associated with negative SST anomalies in the SSCP and enhanced convection not only in the ITCZ over the central equatorial Pacific but also in the SPCZ extended into the subtropical regions of the southeastern Pacific Ocean (Fig. 5). The resulting heating forcing intensifies a localized overturning cell, which in turn provides an additional Rossby wave source in the central extratropical South Pacific, in addition to the typical EN one in the tropical region (Fig. 8). As a consequence, the circulation anomaly field in the central South Pacific presents a strong PSA1-like pattern, characterized by a Rossby wave pattern stretching between the equatorial central Pacific and the SH midlatitudes (Fig. 5c). That related circulation pattern is not present over the extratropical South Pacific during EN events associated with warm surface ocean conditions in the SSCP and inactive SPCZ (WW) (Fig. 6).

The basic features that characterize the differences in the response to EN over the South Pacific were identified through the exploration of either the SST conditions in the SSCP (Fig. 3) or the SPCZ activity (Fig. 9). However, the lagged correlations between the SPCZ index and the SST anomalies over SSCP during EN events are larger and significant when the SPCZ activity index leads (Table 2b). That would indicate that the differences in the EN response over the SH might be mainly driven by atmospheric changes, which induces extratropical SST anomalies. Nevertheless, the extent to which SST anomalies in the SSCP are induced by the atmospheric response to ENSO or result from ocean processes independent of ENSO is not fully clear yet. The processes responsible for their generation as well as their feedback on the SPCZ and the atmosphere circulation deserve further exploration.

The differences in the circulation anomalies that characterize both types of EN response over the SH were further explored through the analysis of the activity of the three leading modes of circulation variability. Circulation anomalies in WC compared to those in WW are associated with a more intense PSA1 pattern extended over the central Pacific with a secondary contribution of the HLM and PSA2 patterns. In particular, the differences in the circulation response over the SH during EN seem to be influenced by the interdecadal variability detected in the Pacific by many studies (Zhang et al. 1997 and references therein). Our results show that during austral spring this interdecadal mod-

ulation is mainly evident through changes of the HLM activity.

It is finally worthwhile to point out that the differences between either the SST conditions in the SSCP or the SPCZ activity among EN events during austral spring are associated with significant precipitation changes over southeastern South America (not shown) in agreement with BS2002. Although the current analysis is not intended to be directly applied to prediction, our results certainly contribute to a better identification of precursors for statistical seasonal predictions and they can be relevant to perform a more profound analysis of general circulation model misrepresentations of the EN response over the SH.

Acknowledgments. We gratefully acknowledge the comments of the editor Dr. Siegfried Schubert. We also thank the two anonymous reviewers for their helpful observations and suggestions. This work was supported by the Inter-American Institute for Global Change (CRN-055), University of Buenos Aires (X072), and ANPCyT (PICTs 99-76355 and 07-09950). NCEP–NCAR reanalyses were made available through the Climate Diagnostic Center (http://www.cdc.noaa.gov).

REFERENCES

Alexander, M., I. Bladé, M. Newman, J. Lanzante, N.-C. Lau, and J. Scott, 2002: The atmospheric bridge: The influence of ENSO teleconnections on air–sea interactions over the global oceans. *J. Climate,* **15,** 2205–2231.

Barlow, M., S. Nigam, and E. H. Berbery, 2001: ENSO, Pacific decadal variability, and U.S. summertime precipitation, drought, and streamflow. *J. Climate,* **14,** 2105–2128.

Barros, V. R., and G. E. Silvestri, 2002: The relationship between sea surface temperature at the subtropical south-central Pacific and precipitation in southeastern South America. *J. Climate,* **15,** 251–267.

Berbery, E. H., J. Nogues-Paegle, and J. D. Horel, 1992: Wavelike Southern Hemisphere extratropical teleconnections. *J. Atmos. Sci.,* **49,** 155–157.

Brahmananda Rao, V., S. R. Chapa, J. P. R. Fernandez, and S. H. Franchito, 2002: A diagnosis of rainfall over South America during the 1997/98 El Niño event. Part II: Roles of water vapor transport and stationary waves. *J. Climate,* **15,** 513–522.

Cai, W., and I. G. Watterson, 2002: Modes of interannual variability of the Southern Hemisphere circulation simulated by the CSIRO climate model. *J. Climate,* **15,** 1159–1174.

Garreaud, R. D., and D. S. Battisti, 1999: Interannual (ENSO) and interdecadal (ENSO-like) variability in the Southern Hemisphere. *J. Climate,* **12,** 2113–2123.

Graham, N. E., 1994: Decadal-scale climate variability in the 1970s and 1980s: Observations and model results. *Climate Dyn.,* **10,** 135–162.

Grimm, A. M., V. R. Barros, and M. Doyle, 2000: Climate variability in southern South America associated with El Niño and La Niña events. *J. Climate,* **13,** 35–58.

Hoerling, M. P., A. Kumar, and M. Zhong, 1997: El Niño, La Niña, and the nonlinearity of their teleconnections. *J. Climate,* **10,** 1769–1786.

Hurrell, J. W., and K. E. Trenberth, 1999: Global sea-surface temperature analyses: Multiple problems and their implications for climate analysis, modeling, and reanalysis. *Bull. Amer. Meteor. Soc.,* **80,** 2661–2678.

Kalnay, E., and Coauthors, 1996: The NCEP/NCAR 40-Year Reanalysis Project. *Bull. Amer. Meteor. Soc.,* **77,** 437–471.

Karoly, D. J., 1989: Southern Hemisphere circulation features associated with El Niño–Southern Oscillation events. *J. Climate,* **2,** 1239–1252.

Kidson, J. W., 1999: Principal modes of Southern Hemisphere low-frequency variability obtained from NCEP–NCAR reanalysis. *J. Climate,* **12,** 2808–2830.

——, M. J. Revell, B. Bhaskaran, A. B. Mullan, and J. A. Renwick, 2002: Convection patterns in the tropical Pacific and their influences on the atmospheric circulation at higher latitudes. *J. Climate,* **15,** 137–159.

Kiladis, G. N., and K. C. Mo, 1998: Interannual and intraseasonal variability in the Southern Hemisphere. *Meteorology of the Southern Hemisphere, Meteor. Monogr.,* No. 49, Amer. Meteor. Soc., 307–336.

Kistler, R., and Coauthors, 2001: The NCEP–NCAR 50-year reanalysis: Monthly means CD-ROM and documentation. *Bull. Amer. Meteor. Soc.,* **82,** 247–268.

Kodama, Y.-M., 1999: Roles of the atmospheric heat sources in maintaining the subtropical convergence zones: An aqua-planet GCM study. *J. Atmos. Sci.,* **56,** 4032–4049.

Kumar, A., and M. P. Hoerling, 1997: Interpretation and implications of the observed inter-El Niño variability. *J. Climate,* **10,** 83–91.

Kutzbach, J. E., 1967: Empirical eigenvectors of sea-level pressure, surface temperature and precipitation complexes over North America. *J. Appl. Meteor.,* **6,** 791–802.

Larkin, N. K., and D. E. Harrison, 2001: Tropical Pacific ENSO cold events, 1946–95: SST, SLP, and surface wind composite anomalies. *J. Climate,* **14,** 3904–3931.

Mo, K. C., 2000: Relationships between low-frequency variability in the Southern Hemisphere and sea surface temperature anomalies. *J. Climate,* **13,** 3599–3620.

Montecinos, A., A. Diaz, and P. Aceituno, 2000: Seasonal diagnostic and predictability of rainfall in subtropical South America based on tropical Pacific SST. *J. Climate,* **13,** 746–758.

Plumb, R. A., 1985: On the three-dimensional propagation of stationary waves. *J. Atmos. Sci.,* **42,** 217–229.

Rasmusson, E. M., and K. Mo, 1993: Linkages between 200-mb tropical and extratropical circulation anomalies during the 1986–1989 ENSO cycle. *J. Climate,* **6,** 595–616.

Rayner, N. A., E. B. Horton, D. E. Parker, C. K. Folland, and R. B. Hackett, 1996: A version 2.2 of the global sea-ice and sea surface temperature data set, 1903–1994. Hadley Centre for Climate Prediction and Research Tech. Note 74, 42 pp. [Available online at http://podaac.jpl.nasa.gov.]

Renwick, J. A., 1998: ENSO-related variability in the frequency of South Pacific blocking. *Mon. Wea. Rev.,* **126,** 3117–3123.

Reynolds, R. W., and T. M. Smith, 1994: Improved global sea surface temperature analyses using optimum interpolation. *J. Climate,* **7,** 929–948.

Ropelewski, C. H., and S. Halpert, 1987: Global and regional scale precipitation patterns associated with the El Niño–Southern Oscillation. *Mon. Wea. Rev.,* **115,** 1606–1626.

Sardeshmukh, P. D., and B. J. Hoskins, 1988: The generation of global rotational flow by steady idealized tropical divergence. *J. Atmos. Sci.,* **45,** 1228–1251.

——, G. P. Compo, and C. Penland, 2000: Changes of probability associated with El Niño. *J. Climate,* **13,** 4268–4286.

Schubert, S. D., and C.-K. Park, 1991: Low-frequency intraseasonal tropical–extratropical interactions. *J. Atmos. Sci.,* **48,** 629–650.

Thompson, D. W. J., and J. M. Wallace, 2000: Annular modes in the extratropical circulation. Part I: Month-to-month variability. *J. Climate,* **13,** 1000–1016.

——, ——, and G. C. Hegerl, 2000: Annular modes in the extratropical circulation. Part I: Month-to-month variability. *J. Climate,* **13,** 1018–1036.

Trenberth, K. E., 1993: The different flavors of El Niño. *Proc. 18th Annual Climate Diagnostic Workshop,* Boulder, CO, National Oceanic and Atmospheric Administration, 50–53.

——, and J. Caron, 2000: The Southern Oscillation revisited: Sea level pressure, surface temperatures, and precipitation. *J. Climate*, **13,** 4358–4365.
——, ——, D. Stepaniak, and S. Worley, 2002: Evolution of El Niño–Southern Oscillation and global atmospheric surface temperatures. *J. Geophys. Res.*, **107**, 4065, doi:10.1029/2000JD000298.
Zhang, Y., J. M. Wallace, and D. S. Battisti, 1997: ENSO-like interdecadal variability: 1900–93. *J. Climate*, **10,** 1004–1020.